

Sequential quantum teleportation of optical coherent states

Hidehiro Yonezawa and Akira Furusawa

*Department of Applied Physics, School of Engineering, The University of Tokyo, 7-3-1 Hongo, Bunkyo-ku, Tokyo 113-8656, Japan
and CREST, Japan Science and Technology (JST) Agency, 1-9-9 Yaesu, Chuo-ku, Tokyo 103-0028, Japan*

Peter van Loock

National Institute of Informatics, 2-1-2 Hitotsubashi, Chiyoda-ku, Tokyo 101-8430, Japan

(Received 21 May 2007; published 6 September 2007)

We demonstrate a sequence of two quantum teleportations of optical coherent states, combining two high-fidelity teleporters for continuous variables. In our experiment, the individual teleportation fidelities are evaluated as $F_1=0.70\pm 0.02$ and $F_2=0.75\pm 0.02$, while the fidelity between the input and the sequentially teleported states is determined as $F^{(2)}=0.57\pm 0.02$. This still exceeds the optimal fidelity of one half for classical teleportation of arbitrary coherent states and almost attains the value of the first (unsequential) quantum teleportation experiment with optical coherent states.

DOI: [10.1103/PhysRevA.76.032305](https://doi.org/10.1103/PhysRevA.76.032305)

PACS number(s): 03.67.Hk, 03.67.Mn, 42.50.Dv, 03.67.Lx

I. INTRODUCTION

By utilizing shared entanglement and classical communication, quantum teleportation [1] enables one, in principle, to transfer arbitrary quantum states with unit fidelity. In a realistic scenario, typically, a receiver obtains an imperfect version of the sender's state. If the receiver decides to teleport his approximate version to a third party, the original quantum state will further degrade when it arrives at the final destination. Such a sequential quantum teleportation therefore requires a sufficiently good performance of each individual teleporter; otherwise the finally teleported state would hardly resemble the input state.

Most protocols for quantum information processing and their experimental realizations are based upon either discrete qubits (qudits) or continuous phase-space variables. In quantum optical implementations, typically, the single-photon-based qubit approach suffers from rather low efficiencies, but achieves, in principle, near-unit fidelities. Combining several single-photon teleporters [2,3] would, in principle, still result in very good fidelities, though conditioned upon coinciding detection events at very low success rates.

Conversely, when Gaussian resource states and continuous-variable homodyne measurements are used, unconditional operations lead to, in principle, near-unit efficiencies, even when basic subroutines such as quantum teleportation are concatenated. The continuous-variable approach [4–6], however, as it relies on intrinsically imperfect squeezed-state entanglement, will never result in arbitrarily high fidelities. In continuous-variable (CV) quantum teleportation [7], the teleported state is a noisy replica of the input state, with an excess noise depending on the quality of the squeezing and entanglement resources. Therefore, when quantum information is sequentially manipulated through Gaussian resources, for instance, via a sequence of teleportation circuits in a continuous-variable cluster computation [8], the unwanted excess noise accumulates and leads to increasingly deteriorating fidelities. In order to achieve still better than classical fidelities, it is thus crucial to improve the quality of each individual teleporter.

So far, a variety of (unsequential) quantum teleportation protocols have been demonstrated, for instance, with photo-

nic qubits [2,3], optical field modes [9], between atoms [10,11], and even between light and atoms [12]. Since the first realization of CV quantum teleportation of optical coherent states [9], several related experiments have followed [12–17]. The CV quantum teleporter can be characterized by the fidelity $F=\langle\psi|\hat{\rho}_{\text{out}}|\psi\rangle$ for an input state $|\psi\rangle$ and a teleported state $\hat{\rho}_{\text{out}}$. Furthermore, in order to assess the performance of the teleporter, we have to determine the fidelity averaged over all possible input states [18]. When the quantum information to be transferred is encoded onto a coherent state drawn from an alphabet of arbitrary coherent states, the gains of the classical channels should be set to unity to maximize the average fidelity (F_{av}). In the case of teleportation of coherent states with unit gains, the average fidelity is identical to the fidelity for a particular coherent state input ($F=F_{\text{av}}$) [16]. The total (average) fidelity for a sequence of n quantum teleportations may then be described by [19]

$$F^{(n)}=1/(1+ne^{-2r}), \quad (1)$$

where r is the squeezing parameter of the (equally) entangled, standard two-mode squeezed-state resources. In the case of $n=2$, at least $r=0.35$ is required (corresponding to two $F=2/3$ teleporters) in order to surpass the classical limit $F_{\text{cl}}=1/2$ [18,20,21].

In the present work, we demonstrate an experiment of two sequential quantum teleportations of optical coherent states. The input states are teleported from a sender (“Alice 1”) to a first receiver (“Bob 1”) and could be retrieved there, as we verify through fidelity measurements. In a second round of teleportation, the output states of the first teleporter are then transferred from Bob 1 (now acting as “Alice 2”) to a second receiver (“Bob 2”) where they can be verified again via fidelity measurements. As we use two high-fidelity teleporters, the total fidelity of the output states is still well beyond the classical limit, despite the excess noise accumulated during the two rounds of quantum teleportation. During the entire protocol, none of the participants (the Alice's and Bob's) gain any substantial information about the input state, though they do obtain some partial knowledge because of the non-

maximal degree of entanglement of the finitely squeezed states used for teleportation.

Based on these results, one could sequentially communicate coherent signal states over two different segments of a channel, provided the corresponding amount of entanglement is available in each channel segment. For realistic, noisy channels, this would require entanglement distillation (purification) procedures [22,23] performed prior to the teleportations. In general, however, by dividing a communication channel into shorter segments [24], a higher degree of entanglement can be maintained in each segment and entanglement distillation will be more efficient. Via sequential quantum teleportation, quantum information can then be sent to an intermediate station where it could be either retrieved or passed on to the next station.

If the total communication channel covers a large distance, it will be necessary to connect some of the purified entangled states via entanglement swapping [25] and repurify the resulting states [24]. Using various levels of purification and swapping enables one to cover a larger distance compared to sequential quantum teleportation. However, after entanglement swapping, quantum information can no longer be transferred to the intermediate stations and potentially retrieved there. As a consequence, in CV entanglement swapping [15], resource requirements are less demanding and, in principle, any nonzero squeezing value of the initial two-mode squeezed states results in a swapped entangled state sufficient for $F > F_{\text{cl}} = 1/2$ quantum teleportation of coherent states [26] (as opposed to the $r > 0.35$ squeezing limit in sequential quantum teleportation). A comparison between these related schemes is shown in Fig. 1.

Concerning quantum computation rather than communication, measurement-based schemes [27–29] have been shown to be an interesting alternative to the more traditional circuit-based approach. The present experiment is also a first step towards a sequential, measurement-based manipulation of quantum information during its propagation through an efficient Gaussian resource state [8,30]. A comparison of the current sequential teleportation scheme with a protocol in which an input state is sent through a linear Gaussian cluster state is shown in Fig. 1.

II. SEQUENTIAL QUANTUM TELEPORTATION PROTOCOL

The quantum state to be teleported here is that of an electromagnetic field mode. An electromagnetic field mode is represented by an annihilation operator \hat{a} with real and imaginary parts \hat{x} and \hat{p} corresponding to the “position” and “momentum” quadrature-phase amplitude operators. These operators \hat{x} and \hat{p} satisfy the commutation relation $[\hat{x}, \hat{p}] = i/2$ (units-free, with $\hbar = 1/2$).

In our experiment, the input state is a coherent state for an optical sideband at 1 MHz. The experimental setup is shown in Fig. 2. In order to generate squeezed vacuum states, we use four subthreshold optical parametric oscillators (OPOs) with a periodically poled KTiOPO₄ as a nonlinear medium [19]. An output of cw Ti:sapphire laser at 860 nm is frequency doubled in an external cavity with a potassium ni-

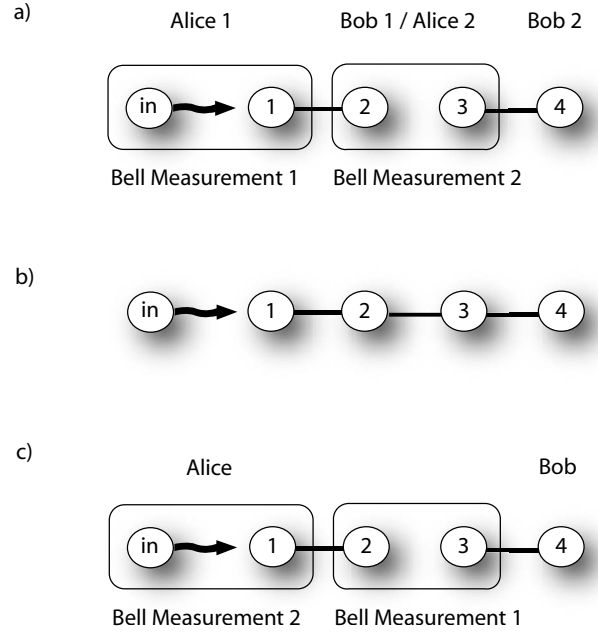


FIG. 1. Comparison of sequential quantum teleportation (a) with the propagation of a quantum state through a linear cluster state (b) and entanglement swapping plus quantum teleportation (c). In the present experiment, the input coherent state is first teleported onto mode 2 as in (a); after this first quantum teleportation, the input state, now present in mode 2, could be verified by measuring its fidelity; the state of mode 2 is then again teleported, this time onto mode 4. In the cluster scenario (b), the input state is attached to the cluster and, in order to send it along the chain to mode 4, quadrature measurements are performed on each individual mode except mode 4; the entangling gate, attaching the input mode to the cluster, and the subsequent single-mode measurements of the input mode and mode 1 correspond to Bell measurement 1 in (a); however, different than (a), in (b), there is no intermediate occurrence of the teleported state at mode 2, as modes 2 and 3 have been entangled *prior* to any measurements; in (a), the entangling gate between 2 and 3 is postponed until Bell measurement 2. Another related scheme is (c), including entanglement swapping; here the first Bell measurement is performed on modes 2 and 3, leaving modes 1 and 4 in an entangled state (whose particular form depends on the measurement outcomes); finally the input state can be teleported onto mode 4 via a second Bell measurement of the input mode and mode 1; again different from (a), in (c), there is no intermediate occurrence of the input state at mode 2.

bate crystal. The output beam at 430 nm is divided into four beams to pump the four OPOs. The pump powers are about 90 mW. By combining two squeezed-vacuum states at a symmetric beam splitter, we can generate an entangled two-mode squeezed (EPR) state. Using four squeezed vacuum states, we generate two pairs of EPR beams in order to construct two teleporters.

In the following, we describe the teleportation process in the Heisenberg representation. Initially, the sender Alice and the receiver Bob share a pair of EPR beams. Alice performs a joint measurement on her EPR mode (\hat{x}_A, \hat{p}_A) and the input mode $(\hat{x}_{\text{in}}, \hat{p}_{\text{in}})$. She combines these two modes at a symmetric beam splitter and measures $\hat{x}_u = (\hat{x}_{\text{in}} - \hat{x}_A)/\sqrt{2}$ and $\hat{p}_v = (\hat{p}_{\text{in}} + \hat{p}_A)/\sqrt{2}$ with two homodyne detectors. The measure-

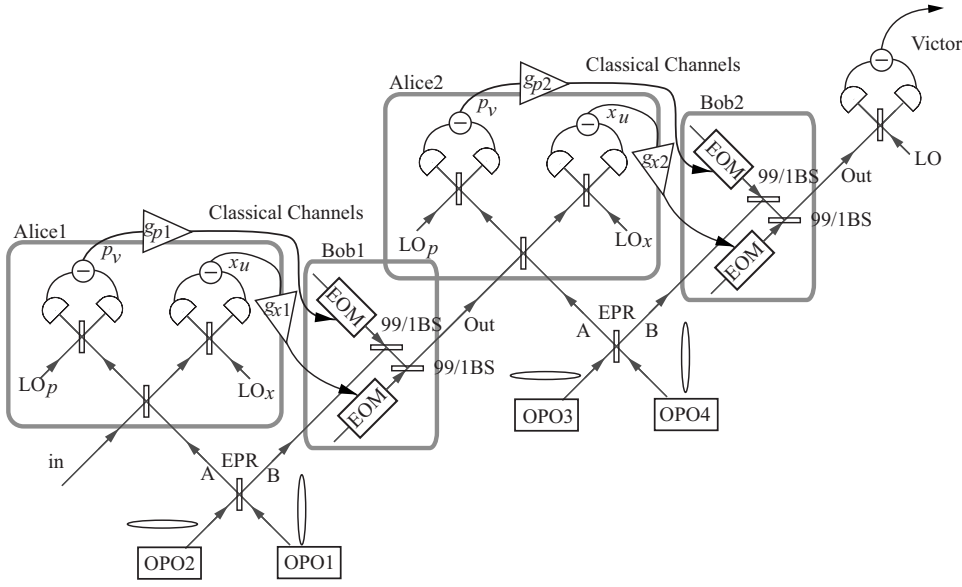


FIG. 2. Experimental setup for sequential quantum teleportation. OPOs are optical parametric oscillators. EOMs are electro-optical modulators. All beam splitters except 99/1 BSs are 50-50 beam splitters. LOs are local oscillators for homodyne detection.

ment results (x_u, p_v) are then sent to Bob through classical channels with gain g_x and g_p .

The (normalized) gains of the classical channels are adjusted similar to Ref. [14] and defined as $g_x = \langle \hat{x}_{\text{out}} \rangle / \langle \hat{x}_{\text{in}} \rangle$, $g_p = \langle \hat{p}_{\text{out}} \rangle / \langle \hat{p}_{\text{in}} \rangle$. The adjusted gains for the teleporters 1 and 2 are $g_{x1} = 1.00 \pm 0.02$, $g_{p1} = 1.00 \pm 0.02$ and $g_{x2} = 1.00 \pm 0.01$, $g_{p2} = 1.00 \pm 0.01$, respectively. For simplicity, these gains are fixed throughout the experiment and treated as unity.

Bob receives Alice's measurement results (x_u, p_v) through the classical channels and displaces his EPR beam (\hat{x}_B, \hat{p}_B) accordingly, $\hat{x}_B \rightarrow \hat{x}_{\text{out}} = \hat{x}_B + \sqrt{2}x_u$ and $\hat{p}_B \rightarrow \hat{p}_{\text{out}} = \hat{p}_B + \sqrt{2}p_v$. In our experiment, the displacement operations are realized via electro-optical modulators (EOMs) and highly reflecting mirrors (99/1 beam splitters). Bob modulates two beams by using amplitude and phase modulators, corresponding to the displacement of x and p quadratures, respectively. The modulated beams are combined with Bob's mode (\hat{x}_B, \hat{p}_B) at the 99/1 beam splitters.

The teleported mode can be written as [15]

$$\hat{x}_{\text{out}} = \hat{x}_{\text{in}} - (\hat{x}_A - \hat{x}_B), \quad \hat{p}_{\text{out}} = \hat{p}_{\text{in}} + (\hat{p}_A + \hat{p}_B). \quad (2)$$

Ideally, the EPR beams would have perfect correlations such that $\hat{x}_A - \hat{x}_B \rightarrow 0$ and $\hat{p}_A + \hat{p}_B \rightarrow 0$. Hence, the state of the output mode, expressed by \hat{x}_{out} and \hat{p}_{out} , would coincide with that of the input mode, \hat{x}_{in} and \hat{p}_{in} .

III. EXPERIMENTAL RESULTS

In the real experiment, the teleported state has some additional noise due to the finite EPR correlations, i.e., $\Delta_{\text{EPR}}(x) \equiv \langle [\Delta(\hat{x}_A - \hat{x}_B)]^2 \rangle \neq 0$ and $\Delta_{\text{EPR}}(p) \equiv \langle [\Delta(\hat{p}_A + \hat{p}_B)]^2 \rangle \neq 0$. In the process of n sequential quantum teleportations, this excess noise is added n times to the input state. Thus, the variances of the output state are

$$\langle (\Delta \hat{x}_{\text{out}}^{(\text{seq})})^2 \rangle = \langle (\Delta \hat{x}_{\text{in}})^2 \rangle + \sum_i \Delta_{\text{EPR},i}(x),$$

$$\langle (\Delta \hat{p}_{\text{out}}^{(\text{seq})})^2 \rangle = \langle (\Delta \hat{p}_{\text{in}})^2 \rangle + \sum_i \Delta_{\text{EPR},i}(p), \quad (3)$$

where $\Delta_{\text{EPR},i}$ are the added noise terms of the i th teleporter.

Figure 3 shows the measurement results of the two sequential quantum teleportations. The outputs of the homodyne detection are measured by a spectrum analyzer. The measurement frequency is 1 MHz. Figure 3(a) shows the input coherent state with the phase scanned. In our experiment, an input coherent state is generated by modulating a weak coherent beam at 1 MHz. Figure 3(b) shows the teleported states for the x quadrature (the p quadrature is not shown). The variances of the teleported state are $\langle (\Delta \hat{x}_{\text{out}}^{(1)})^2 \rangle = 2.5 \pm 0.2$ dB and $\langle (\Delta \hat{p}_{\text{out}}^{(1)})^2 \rangle = 2.8 \pm 0.2$ dB relative to the vacuum noise level. Here superscript (1) stands for the output of the first teleporter. Figure 3(c) shows sequentially teleported states for the x quadrature (the p quadrature is not shown). The variances of the sequentially teleported state are $\langle (\Delta \hat{x}_{\text{out}}^{(\text{seq})})^2 \rangle = 3.9 \pm 0.2$ dB and $\langle (\Delta \hat{p}_{\text{out}}^{(\text{seq})})^2 \rangle = 4.0 \pm 0.2$ dB. Note that the amplitudes of the teleported states are almost identical to those of the input states, reassuring that the gains of the teleporters are near unity.

We also evaluate the performance of the second teleporter individually (not shown in Fig. 3). We teleport a coherent state by using the second teleporter, and determine the variances of the output. The measured variances of the output state are $\langle (\Delta \hat{x}_{\text{out}}^{(2)})^2 \rangle = 2.3 \pm 0.2$ dB and $\langle (\Delta \hat{p}_{\text{out}}^{(2)})^2 \rangle = 2.2 \pm 0.2$ dB with respect to the vacuum noise level. From Eq. (3), we can calculate the variance of the sequentially teleported state from the added noise of each teleporter. The calculated variances are $\langle (\Delta \hat{x}_{\text{out}}^{(\text{seq})})^2 \rangle = 3.9$ dB and $\langle (\Delta \hat{p}_{\text{out}}^{(\text{seq})})^2 \rangle = 4.1$ dB, which is in good agreement with the experimental results. This confirms that our teleporters maintain their fidelities even when combining them. In principle, we can build a larger sequence of teleporters (though at the expense of a further decreasing total fidelity).

To estimate the performance of a teleporter, we use the fidelity $F = \langle \alpha | \hat{\rho}_{\text{out}} | \alpha \rangle$ for teleporting a coherent state with

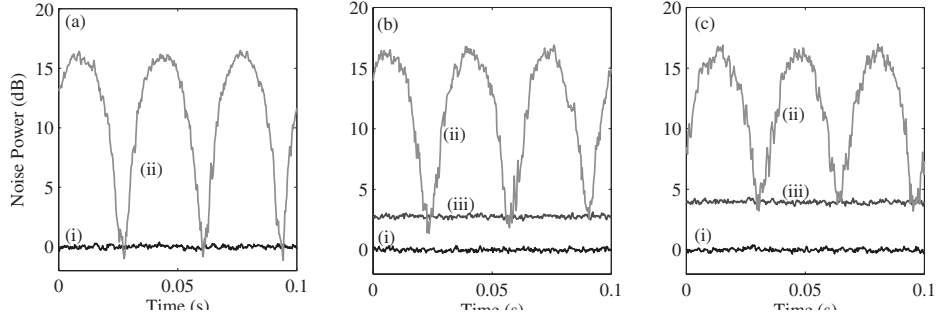


FIG. 3. Measurement results of sequential teleportation for x quadrature (p quadrature is not shown). In all figures, traces (i) show vacuum noise level. (a) Input coherent state. Trace (ii) shows the input state with phase scanned. (b) Teleported states for x quadrature. Trace (ii) shows the teleported states for a coherent state input with a phase of the input state scanned. Trace (iii) shows the teleported states for a vacuum input of which noise level corresponds to the variances of the output. The variance is 2.5 ± 0.2 dB (that of p is 2.8 ± 0.2 dB). (c) Sequentially teleported state. Trace (ii) shows sequentially teleported states for a coherent state input. Trace (iii) show the sequentially teleported states for a vacuum input. The variance is 3.9 ± 0.2 dB (that of p is 4.0 ± 0.2 dB). The measurement frequency is 1 MHz, resolution and video bandwidths are 30 kHz and 300 Hz, respectively. All traces except for (ii) are averaged 30 times.

amplitude α yielding the output state $\hat{\rho}_{\text{out}}$. For coherent-state inputs with unity gains, the fidelity can be written as [15]

$$F = \frac{2}{\sqrt{[1 + 4\langle(\Delta\hat{x}_{\text{out}})^2\rangle][1 + 4\langle(\Delta\hat{p}_{\text{out}})^2\rangle]}}. \quad (4)$$

The fidelity is calculated from the variances of the output states. The variances of the coherent state input is $\langle(\Delta\hat{x}_{\text{in}})^2\rangle = \langle(\Delta\hat{p}_{\text{in}})^2\rangle = 1/4$, hence the fidelity can be determined by the added noise of $\Delta_{\text{EPR}}(x)$ and $\Delta_{\text{EPR}}(p)$. We calculate the fidelity from the measured variances using Eq. (4). The performance of each teleporter is estimated for a coherent-state input as $F_1 = 0.70 \pm 0.02$ and $F_2 = 0.75 \pm 0.02$ for teleporters 1 and 2, respectively. Note that our teleporters exceed both the classical limit $F_{\text{cl}} = 1/2$ [18,20,21] and the no-cloning limit $F_{\text{NC}} = 2/3$ [31,32]. We also calculate the fidelity between the input and the sequentially teleported state. The fidelity is $F^{(2)} = 0.57 \pm 0.02$ which still exceeds the classical limit $F_{\text{cl}} = 1/2$ and verifies the successful demonstration of two sequential quantum teleportations.

Figure 4 shows the Wigner functions reconstructed via

optical homodyne tomography technique [33]. The Wigner function is a quasiprobability distribution defined by $W(x, p) = \frac{2}{\pi} \int d\xi \exp(-4i\xi p) \langle x + \xi | \hat{\rho} | x - \xi \rangle$ [34,33]. In optical homodyne tomography, we also use 1 MHz sidebands of the carrier beam [35]. The output of a homodyne detector is high-pass filtered and then mixed with an electrical oscillator signal of frequency 1 MHz, which is the same frequency as for the creation of the input coherent state. The intermediate-frequency output of the mixer is low-pass filtered (the bandwidth is 30 kHz) and recorded in a PC with an analog-to-digital converter (ADC). The sampling rate of the ADC is set to 300 kHz and we measure around 100 000 points with the local oscillator (LO) phase scanned. To reconstruct the Wigner function, we use the inverse Radon transformation [33,35]. Figure 4(a) shows the input coherent state. Figure 4(b) shows the teleported state, and Fig. 4(c) shows the sequentially teleported state. Note that here we lock the phase of the input coherent state to $\sim 45^\circ$ with respect to the x quadrature. Although the teleported states have excess noise and turn into mixed states, the input state is clearly reconstructed after the two rounds of quantum teleportation.

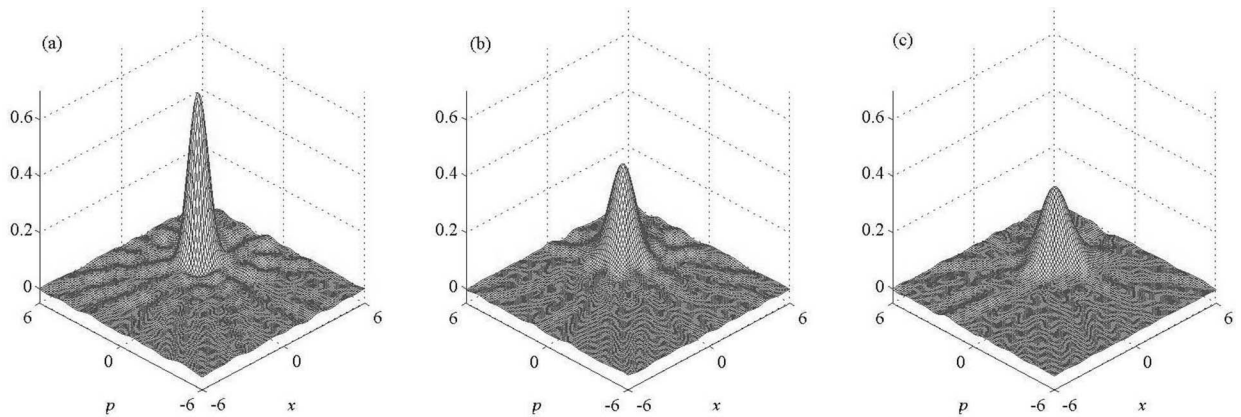


FIG. 4. Wigner function reconstructed by using optical homodyne tomography. (a) Input coherent state. (b) Teleported state. (c) Sequentially teleported state. In these measurement, we locked the phase of input coherent state $\sim 45^\circ$ from x quadrature.

IV. SUMMARY

In summary, we demonstrated two sequential quantum teleportations of coherent states of light. The experimentally determined fidelity for the sequentially teleported coherent states was well beyond the classical limit. These results imply the possibility of sequential quantum communication over several segments of a channel using efficient Gaussian resources (combined with non-Gaussian distillation techniques [23]). Moreover, our experiment represents a step towards sequentially manipulating quantum information using

entangled Gaussian resource states. Future extensions of this work will include more general measurement-based Gaussian transformations [30] and the use of non-Gaussian signal states as well as the addition of non-Gaussian measurements in order to achieve universal quantum information processing [8].

ACKNOWLEDGMENTS

This work was partly supported by the MEXT of Japan.

-
- [1] C. H. Bennett, G. Brassard, C. Crepeau, R. Jozsa, A. Peres, and W. K. Wootters, *Phys. Rev. Lett.* **70**, 1895 (1993).
 - [2] D. Bouwmeester, J.-W. Pan, K. Mattle, M. Eibl, H. Weinfurter, and A. Zeilinger, *Nature (London)* **390**, 575 (1997).
 - [3] D. Boschi, S. Branca, F. De Martini, L. Hardy, and S. Popescu, *Phys. Rev. Lett.* **80**, 1121 (1998).
 - [4] S. L. Braunstein and A. K. Pati, *Quantum Information with Continuous Variables* (Kluwer Academic Publishers, Dordrecht, 2003).
 - [5] S. L. Braunstein and P. van Loock, *Rev. Mod. Phys.* **77**, 513 (2005).
 - [6] J. Eisert and M. B. Plenio, *Int. J. Quantum Inf.* **1**, 479 (2003).
 - [7] S. L. Braunstein and H. J. Kimble, *Phys. Rev. Lett.* **80**, 869 (1998).
 - [8] N. C. Menicucci, P. van Loock, M. Gu, C. Weedbrook, T. C. Ralph, and M. A. Nielsen, *Phys. Rev. Lett.* **97**, 110501 (2006).
 - [9] A. Furusawa, J. L. Sørensen, S. L. Braunstein, C. A. Fuchs, H. J. Kimble, and E. S. Polzik, *Science* **282**, 706 (1998).
 - [10] M. Riebe, H. Häffner, C. F. Roos, W. Hänsel, J. Benhelm, G. P. T. Lancaster, T. W. Körber, C. Becher, F. Schmidt-Kaler, D. F. V. James, and R. Blatt, *Nature (London)* **429**, 734 (2004).
 - [11] M. D. Barrett, J. Chiaverini, T. Schaetz, J. Britton, W. M. Itano, J. D. Jost, E. Knill, C. Langer, D. Leibfried, R. Ozeri, and D. J. Wineland, *Nature (London)* **429**, 737 (2004).
 - [12] J. F. Sherson, H. Krauter, R. K. Olsson, B. Julsgaard, K. Hammerer, I. Cirac, and E. S. Polzik, *Nature (London)* **443**, 557 (2006).
 - [13] W. P. Bowen, N. Treps, B. C. Buchler, R. Schnabel, T. C. Ralph, Hans-A. Bachor, T. Symul, and P. K. Lam, *Phys. Rev. A* **67**, 032302 (2003).
 - [14] T. C. Zhang, K. W. Goh, C. W. Chou, P. Lodahl, and H. J. Kimble, *Phys. Rev. A* **67**, 033802 (2003).
 - [15] N. Takei, H. Yonezawa, T. Aoki and A. Furusawa, *Phys. Rev. Lett.* **94**, 220502 (2005).
 - [16] H. Yonezawa, T. Aoki, and A. Furusawa, *Nature (London)* **431**, 430 (2004).
 - [17] N. Takei, T. Aoki, S. Koike, K. Yoshino, K. Wakui, H. Yonezawa, T. Hiraoka, J. Mizuno, M. Takeoka, M. Ban, and A. Furusawa, *Phys. Rev. A* **72**, 042304 (2005).
 - [18] S. L. Braunstein, C. A. Fuchs, and H. J. Kimble, *J. Mod. Opt.* **47**, 267 (2000).
 - [19] S. Suzuki, H. Yonezawa, F. Kannari, M. Sasaki, and A. Furusawa, *Appl. Phys. Lett.* **89**, 061116 (2006).
 - [20] S. L. Braunstein, C. A. Fuchs, H. J. Kimble, and P. van Loock, *Phys. Rev. A* **64**, 022321 (2001).
 - [21] K. Hammerer, M. M. Wolf, E. S. Polzik, and J. I. Cirac, *Phys. Rev. Lett.* **94**, 150503 (2005).
 - [22] C. H. Bennett, G. Brassard, S. Popescu, B. Schumacher, J. A. Smolin, and W. K. Wootters, *Phys. Rev. Lett.* **76**, 722 (1996).
 - [23] D. E. Browne, J. Eisert, S. Scheel, and M. B. Plenio, *Phys. Rev. A* **67**, 062320 (2003).
 - [24] H.-J. Briegel, W. Dür, J. I. Cirac, and P. Zoller, *Phys. Rev. Lett.* **81**, 5932 (1998).
 - [25] M. Zukowski, A. Zeilinger, M. A. Horne, and A. K. Ekert, *Phys. Rev. Lett.* **71**, 4287 (1993).
 - [26] P. van Loock and S. L. Braunstein, *Phys. Rev. A* **61**, 010302(R) (1999).
 - [27] M. A. Nielsen, *Rep. Math. Phys.* **57**, 147 (2006).
 - [28] R. Raussendorf and H. J. Briegel, *Phys. Rev. Lett.* **86**, 5188 (2001).
 - [29] D. Gottesman and I. L. Chuang, *Nature (London)* **402**, 390 (1999).
 - [30] P. van Loock, *J. Opt. Soc. Am. B* **24**, 340 (2007).
 - [31] N. J. Cerf, A. Ipe, and X. Rottenberg, *Phys. Rev. Lett.* **85**, 1754 (2000).
 - [32] F. Grosshans and P. Grangier, *Phys. Rev. A* **64**, 010301(R) (2001).
 - [33] U. Leonhardt, *Measuring the Quantum State of Light* (Cambridge University Press, Cambridge, 1997).
 - [34] E. P. Wigner, *Phys. Rev.* **40**, 749 (1932).
 - [35] G. Breitenbach and S. Schiller, *J. Mod. Opt.* **44**, 2207 (1997).